

Article



3D printable regolith filled shape memory vitrimer composite for extraterrestrial application

Journal of Composite Materials 2024, Vol. 58(24) 2639–2654 © The Author(s) 2024 Article reuse guidelines: sagepub.com/journals-permissions DOI: 10.1177/00219983241274544 journals.sagepub.com/home/jcm



Kingsley Yeboah Gyabaah¹, John Konlan², Obed Tetteh¹, Maryam Jahan³, Enrique Jackson⁴, Patrick Mensah¹ and Guoqiang Li^{1,2}

Abstract

This study investigates a neoteric approach in manufacturing lunar regolith-filled shape memory vitrimer (SMV) composites for extraterrestrial applications. A SMV with robust mechanical properties was combined with locally available lunar regolith to form a composite material. Fourier Transfer Infrared Spectroscopy (FTIR), Scanning Electron Microscope (SEM), Thermogravimetric Analysis (TGA), and X-ray fluorescence (XRF) were used to characterize the resin, the regolith simulant, and the prepared SMV-regolith composites. We explored conventional synthesis as well as 3D printing methods for manufacturing the composite. Glass fabric-reinforced laminated composites were also prepared to evaluate the impact tolerance and damage healing efficiency. Compressive strength, flexural strength, and impact resistance of the composite were tested at both room and elevated temperatures. A compressive strength of 96.0 MPa and 5.4 MPa were recorded for composite with 40 wt% regolith ratio at room and elevated temperatures, respectively. The glass fabric reinforced SMVregolith laminate exhibited a bending strength of 232.7 MPa, good impact tolerance under low-velocity impact test, and good healing efficiency up to two damage healing cycles. The 3D printed SMV-regolith composite using a liquid crystal display (LCD)-based printer exhibited a good thermomechanical property with a compressive and tensile strength of 139.16 MPa and 13.99 MPa, respectively, and a good shape memory effect. However, the LCD-based printing using vatphotopolymerization limits the size of the printed samples. Nonetheless, this study shows that utilization of regolith to form advanced composite is possible. SMV regolith composite is a promising material for lunar base applications due to its simple manufacturing process, excellent mechanical properties, and low energy consumption.

Keywords

shape memory vitrimer, regolith, 3D printing, low-velocity impact, self-healing

Introduction

Developing an independent extraterrestrial settlement has for decades been a staple of science fiction literature. Space exploration is now technically possible because of significant technological advancements over the previous few decades. Being the nearest celestial body to Earth, the Moon is abundant in a variety of minerals and energy sources, including sunlight and helium-3, metals, and ilmenite, which appear to be ideal locations for further deep space exploration and settlement. Space agencies like NASA, ESA, and CNSA have all demonstrated a long-term commitment to lunar base construction and inhabited space exploration. The purpose of establishing extraterrestrial bases and possibly permanent residence on the Moon is to provide protection from meteorite impacts, solar and cosmic radiation, and extreme temperature fluctuations, which

will create the foundation and optimum environment for further deep space colonization. However, one of the

Corresponding author:

Guoqiang Li, Department of Mechanical Engineering, Southern University and A & M College, 801 harden blvd, Baton Rouge, LA 70813, USA. Email: |guoqil@|su.edu

Data Availability Statement included at the end of the article

¹Department of Mechanical Engineering, Southern University and A & M College, Baton Rouge, LA, USA

²Department of Mechanical & Industrial Engineering, Louisiana State University, Baton Rouge, LA, USA

³Department of Chemistry, Southern University and A & M College, Baton Rouge, LA, USA

⁴EM3 I-Materials Science and Metallurgy Branch, NASA-Marshall Space Flight Center, Huntsville, AL, USA

biggest obstacles to lunar colonization is the exorbitant cost of shipping raw materials from Earth to construct both temporary and permanent structures on the Moon. Based on current research, the development of lunar construction has been severely limited by the high cost of transferring source materials and the substantial payload transported from Earth. To continue our exploration and advancement of space, humans will need to identify, extract, and use local resources, much as the exploration of our globe requires us to adapt and learn how to use resources that vary by continent, region, and climate.

For this reason, in-situ resource utilization (ISRU) technology offers a potential remedy for building lunar bases. 13 Expanding human presence on the Moon and throughout the solar system requires learning how to use in situ resources on the Moon.¹⁴ By extending mission durations while minimizing logistics, effective in situ lunar resource utilization for the development of structures, materials, power generation, and other areas can boost mission efficiency and scientific returns. 15 Large-scale onsite manufacturing is needed to accomplish the goal of building a permanent base on a celestial body. On-site manufacturing using in-situ resources is essential for long-term sustainability. In-situ resource utilization will enable the affordable establishment of extraterrestrial exploration and operations by minimizing the materials carried from Earth. Formed from the breakdown of large rocks into smaller particles due to meteorite and micrometeorite. and space weathering, lunar regolith is the main finer fraction of the unconsolidated fragments and material that covers the surface of the Moon. 16,17

Lunar regolith has the potential as a building material or as raw material for construction or industrial-based processes. It has now been demonstrated by numerous researchers to be an easy, feasible, and economical feedstock for lunar construction. ^{18–20} Several research works have been conducted on the use of lunar regolith as raw material for lunar applications. Sintering, concrete, and polymerization are the common methods for consolidating fine regolith particles and forming composite materials with regolith, respectively. Sintering involves the use of heat to consolidate regolith particles into a coherent solid with the help of mass transport at the atomic scale without fully melting the material. 20,21 Sintering of lunar regolith is done by subjecting it to elevated temperature or microwave heating energy of 1200 - 1500 °C¹⁵. The high thermal energy used in the sintering process and the high porosity, cracks, and deformations leading to low mechanical properties of the sintered parts are some of the limitations in the use of sintering as a method of producing construction materials from lunar regolith. 22,23 Research has shown that lunar regolith can also be used as extraterrestrial concrete as a construction material on the Moon.²⁴ Due to its similar chemical composition to cement slag, regolith can also form the ingredient for the development of cementitious construction material. Nonetheless, the requirement for water for the mixing, hydration, and curing of concrete may be the main obstacle preventing concrete from being used as the material of choice for construction in space. Furthermore, the naturally low tensile strength, susceptibility to shrinking, instability, and propensity to outgas under vacuum are further drawbacks. Polymer concrete is another alternative to produce non-hydraulic concrete for space construction. Appropriate polymer binders such as unsaturated polyester, methyl methacrylate, epoxy, polyurethane, and urea-formaldehyde resins have been used to prepare mortar-type, three-dimensional network structures with silicate-based materials.

For instance, Bao et al. worked on the preparation and characterization of elevated and cryogenic temperatureresistant regolith-filled epoxy resin composite. The polymer concrete was formed from a slurry mix of lunar regolith simulant and epoxy-resin-based substrate binder. The mixture was cured in air and at elevated temperatures to form a high-strength three-dimensional network polymer concrete. The performance of the polymer concrete was examined both at room temperature and at elevated temperatures. Furthermore, Lee et al.^{27,28} worked on the manufacturing of polymer concrete on the Moon using thermoplastic polymer and lunar soil under a lunar mimic environment. Polymer concrete was cast from a thermoplastic polymer and lunar soil simulant under vacuum conditions and temperature variation between 20 and 123 °C. The performance of the concrete is proportional to the preheating time of the polymer regolith mix in a mold and the pores in concrete because of an incomplete reaction. In another study, Lee et al.²⁶ studied the bottom-up heating method for producing polyethylene lunar concrete in lunar environments. Their work focused on saving heating time and energy in the manufacturing of polymer regolith concrete in a thermal vacuum chamber. The use of thermosets as matrix binders in the polymer concrete contributes significantly to the mechanical properties and the performance of the polymer concrete. Nevertheless, using thermosets as the binder for polymer concrete raises major problems regarding their reprocessability and recycling as they are intrinsically insoluble and infusible. The presence of permanent covalent bonds in the thermoset makes it difficult to reprocess at the end of their lifetime.²⁹ Thermoplastics on the other hand have very weak mechanical properties making them unsuitable for many applications.³⁰ There is a need for economically sustainable waste management and recycling techniques for polymer composite.31 The introduction of reversible covalent adaptable networks (CANs) into polymer structures has led to another class of polymers called vitrimer.³² Vitrimer combines the mechanical resilience of thermosets and the recyclable, and reprocesseable properties of thermoplastics.³³ The composite community

has studied and adopted vitrimers as matrices in different classes of materials due to their unique and multiple properties.³⁴ Developing sustainable materials for space applications is very important since materials used for various applications can be reprocessed and reused again for long periods. This will help humans reduce the cost of lunar construction and help in waste management. Hence the use of vitrimer as the matrix binder in the polymer regolith concrete is highly desired.

Given the hostile lunar and Martian environments, it would be crucial to create robotic, autonomous processing and construction systems that can survey, gather, and process *in-situ* resources to extract or manufacture building materials. Integrating these systems may increase construction speed, uniformity, and crew member safety. 3D printing technology has proven to be one of the autonomous processing and construction techniques that has the potential for space application. 3D printing can be used to accumulate lunar construction materials to produce structures with fixed geometry and precise construction. ³⁵ This technology will help meet the requirements of interplanetary construction on the Moon.

Recent developments in 3D printing have made it feasible to create intricately shaped, multifunctional parts for use on lunar exploration missions. ^{1,36,37} Mixing lunar regolith with other additives is a common way to provide filaments for 3D printing of parts for lunar application. 38,39 Cesaretti et al. 40 reported on 3D printing of lunar regolith simulant using chlorine-based liquid as the binder. A 3D printer of large dimensions was used to manufacture a representative structure composed of a base material with a similar composition as the actual lunar soil. Jakus et al. worked on extrusion-based 3D printing of regolith simulant ink. The ink for the printing was synthesized from lunar regolith, and a binder consisted of evaporant, surfactant, and plasticizer solvent, polylactic-co-glycolic acid. Liu et al. 41 and Dou et al. 42 used lunar regolith simulant slurry made from regolith simulant and photocurable resin to fabricate structures via a vat polymerization process followed by sintering in air.

Even though mixed lunar regolith combinations have been shown to work for 3D printing, future lunar missions will probably still have to overcome numerous obstacles. Firstly, most of the binders used to consolidate the lunar regolith are not recyclable and hence become a challenge in resource-starved environments like space. Furthermore, there is also a need to improve the thermomechanical properties of the printed parts. Recent advancement in 3D printing is the field of printing structures that can change their shape in response to an external stimulus, which is also called 4D printing. Using shape-memory polymer in multimaterial printing, 4D printing makes it possible to produce three-dimensional objects that may change into different three-dimensional structures when heated or cooled to a particular temperature or radiation. 43,44

In this study, we demonstrate a novel approach to the synthesis of sustainable material that exhibits 4Dprintability for extraterrestrial applications. A shape memory vitrimer regolith composite was synthesized using lunar regolith as the main constituent material and a recyclable, shape memory vitrimer (SMV) as the matrix of the composite. Although different methods have been explored and used to consolidate lunar regolith for extraterrestrial use, there have been no reported research works regarding the use of recyclable and self-healing matrix materials for forming composite with lunar regolith. The use of SMV as the matrix of the composite combines the attractive properties of thermoset such as chemical resistance, and good mechanical, and thermal properties with thermoplastics' reprocessability, self-healing ability, and recyclability. The research found that the SMV regolith composite has good mechanical properties at both room and elevated temperatures, high self-healing efficiency, 3D printability, good shape memory effect, and the potential to be used for extraterrestrial applications.

Experimental

Materials and methods

Bisphenol A glycerolate dimethacrylate and 2-hydroxy-4-(2-hydroxyethoxy)-2-methylpropiophenone were obtained from Sigma Aldrich, USA. Lunar Regolith Simulant was purchased from The Exolith Lab. Bidirectional plain woven glass fabric was obtained from Fiberglast Development Corporation, USA. The materials were used as received.

Preparation of SMV regolith composite and glass fabric reinforced laminated composites

In the preparation of the SMV-regolith composite, Bisphenol A glycerolate dimethacrylate (BPAGMA) was used and 2-hydroxy-4-(2-hydroxyethoxy)-2-methylpropiophenone served as the photoinitiator to initiate the free radical polymerization. The SMV serves as the binder of the lunar regolith simulant. For a measured mass of BPAGMA, 3 wt% of the photoinitiator was siphoned via a pipette and added to the monomer. The mixture was stirred in a silicon bath at 90°C for 2 h.

The SMV-regolith composite (SMVRC) was synthesized by varying the weight percentage of the regolith (10 wt%, 20 wt%, 30 wt%, and 40 wt%) in a fixed mass of the SMV matrix. The mixture of the SMV and the regolith simulant was stirred for 10 min. The cylindrical specimen (height = 30 mm and diameter = 14 mm) of the SMV-regolith composites was cured in a UV chamber for 20s. The samples were removed and allowed to cool for 10 min. Scheme 1 shows the preparation steps by two procedures: conventional procedure, and 3D printing. The UV-cured

sample (Figure 1) were post-cured in an oven at 180°C for 3 h.

To prepare the glass fabric reinforced SMV-regolith composite laminate, glass fabric was cut into plys with a square shape of 165 mm by 165 mm. 160g of the BPAGMA monomer was used and 4.95 g of the photo-initiator was siphoned via a pipette and added to the monomer. Lunar Regolith simulant of varied weight percentage was added to the prepared monomer mixture. This was done to obtain a composite with a higher regolith percentage and investigate the effect of the weight fraction of regolith on the properties of the composites. The mixture was thoroughly stirred for 10 min after which all bubbles were completely removed. The homogenous mixture of monomer, photoinitiator, and regolith was used to wet the cut-out fabrics (165 mm × 165 mm) by a hand layup process. The wet fabrics were placed in an aluminum open mold 5.08 mm thickness. In this research, glass fabric of 35% volume fraction was achieved by using 6 plys of glass fabrics in 165 mm × 165 mm × 5.08 mm mold. Two Teflon sheets and two aluminum plates with square dimensions as the open mold frame were used as the covering of the open frame mold. A mold release agent was applied on the surfaces of the mold and allowed to dry off by blowing air around it. Six C-clamps were used to exert pressure on the mold to prevent the liquid mixture from flowing out of the mold. The compressed setup was then sent to an oven and cured at 180°C for 3 h. After curing and demolding, the cured laminate was cut into 152.40 mm × 25.40 mm × 5.08 mm specimens to be used for low-velocity impact and 3-point bending tests. Glass fabric reinforced pure SMV composite laminates were prepared to serve as a reference.

3D printing of vitrimer-regolith composite

In this study, 3D printable and recyclable SMV-regolith composite resin was prepared by mixing Bisphenol A glycerolate dimethacrylate (BPAGMA), Ethyl (2,4,6-trimethylbenzoyl) phenylphosphinate as the photoinitiator, and the lunar regolith simulant as fillers. Bisphenol A glycerolate dimethacrylate was heated at 110°C for 1 h in an oven to make it less viscous for pouring. In this work, 3 % of the photo-initiator Ethyl (2,4,6-trimethylbenzoyl) phenylphosphinate was dissolved in Bisphenol A glycerolate dimethacrylate (BPAGMA). Triethylamine (0.5 wt%) and 1-4-butanediol dimethacrylate (20 wt%) were added to the BPAGMA as a diluent to obtain a resin of good viscosity for 3D printing. The mixture was stirred in a silicon bath at 90°C for 2 h. 20 wt% of 200 mesh-sized regolith was used in the preparation of the mix for the 3D printing. Anycubic Photon Mono 3D Printer was used for LCD-based 3D printing. A 405 nm LED array was used. A bottom exposure time of 45 s, normal exposure time of 0.8 s, UV-power of



Figure 1. Synthesized vitrimer regolith composite samples.

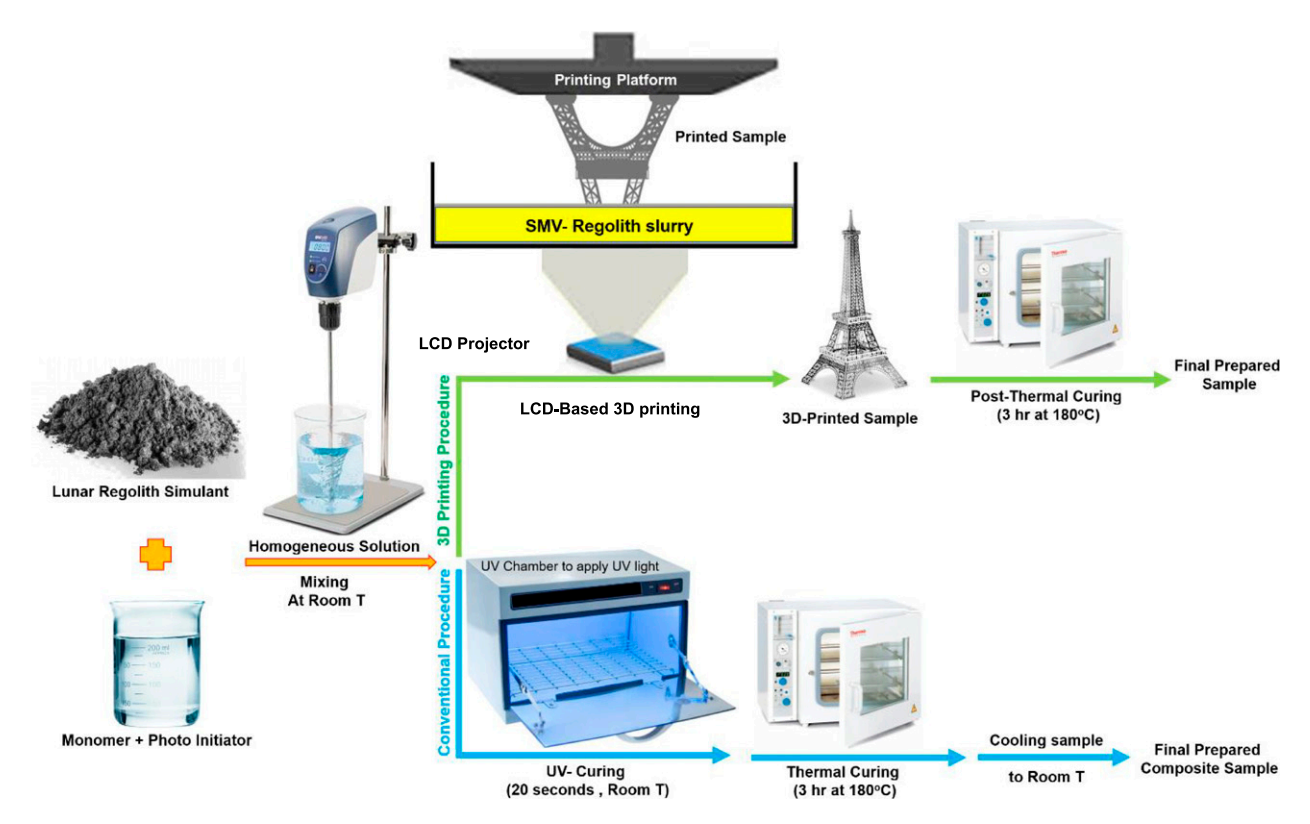
70%, and a printing speed of 800 mm/h are the printing parameters.

Mechanical properties and healing efficiency testing

Cylindrical samples of the control samples without regolith and the composite of different regolith weight fractions (10, 20, 30, and 40 wt%) were polished for compressive testing. At least four effective samples of each composite and control were used for the compressive tests. The compressive behavior of the pure SMV and the composites were investigated at room temperature using an MTS Q150 machine with a loading rate of 1 mm/min.

Low velocity impact test was conducted on the composite laminate using an Instron Dynatup 8250 HV impactor per ASTM D3763-18 standard. The specimen dimension was 152.40 mm × 25.40 mm × 5.08 mm. During the low-velocity impact test, the hammer weight used was 5.6 kg which was dropped from a height of 205 mm, leading to an impact velocity of 2 m/s. The impact location was at the center of the specimen. At least four effective samples were examined for each impact cycle to calculate the average value and the standard deviation. From the impact tests, the maximum impact load, initiation energy, and propagation energy were obtained.

An MTS Alliance RF/10 machine with a loading rate of 2.0 mm/min was used to conduct the 3-point bending test.



Scheme I. Schematic of Preparation of Vitrimer Regolith Composite.

Equation (1) was used to determine the flexural stress at any point on the load-deflection curve that occurs at the bottom surface at the mid-span.

$$\sigma_f = \frac{3PL}{2hh^2} \tag{1}$$

where σ_f = flexural stress at the outer surface at midspan, P = applied force, L = span length, b = beam width, and h = beam thickness.

One of the primary goals of choosing SMV as the matrix for the composite materials is the intrinsic reprocessing and recycling properties of the polymer. The reversible covalent bonds in the vitrimer endow the polymer with these important properties. Li et al. 45 worked on recyclable thermoset SMV where the healing efficiency of the polymer was computed after recycling. Konlan et al. 46,47 demonstrated the self-healing of laminated SMV composites where resistive Joule heating was used to trigger the reconfiguration of broken bonds in the polymer composite after low-velocity impact tests. The healing efficiency can be computed by using ratios of either the Crack Initiation Energy (CIE) or Crack Propagation Energy (CPE) of the composite laminates under the impact tests before and after healing. The healing of the composite was done at a temperature above the glass transition temperature where the transesterification reaction can occur, leading to the recombination of broken bonds.

In this work, the healing of the composite laminate was performed at 150°C, healing pressure of 16 MPa, and a healing time of 2 h. Applying pressure of 16 MPa provided the required healing compressive stress of 14 MPa. After carrying out the first impact test, the SMV-regolith composite laminate was sandwiched between two rectangular stainless-steel plates having the same dimension as the laminate, and the setup was placed in a preheated oven at 150°C for 1 h. A constant healing pressure was then exerted for 2 h. This was done to achieve a higher healing efficiency during the transesterification reaction in the polymer chain. The oven was turned off after 2 h Of healing period and allowed to cool to room temperature. The healing efficiency of the composite laminate was computed based on the crack initiation and propagation energy.

$$I_{HE} = \frac{IE_A}{IE_B} \tag{2}$$

$$P_{HE} = \frac{PE_A}{PE_B} \tag{3}$$

where the notation I_{HE} and P_{HE} represent the healing efficiency of the SMV-regolith composite laminate in terms of crack initiation energy and crack propagation energy,

respectively. IE_A is the crack initiation energy of the composite after healing, and IE_B is the crack initiation energy of the composite before healing. PE_A is the crack propagation energy of the composite after healing, and PE_B is the crack propagation energy of the composite before healing.

Porosity measurement

The densities of the composites with different regolith weight ratios were measured using both standard volumetric displacement methods and calculated from data using an AccuPyc II 1340 Gas Pycnometer. The Pycnometer was used to measure the composite materials' volume and density. Helium gas was used as the inert gas to permeate small pores within the material. Cylindrical-shaped composites were used for porosity measurement. The theoretical densities were determined by using the standard rule of mixtures approach.

The mass of the composites with different regolith ratios was measured and added to a regulated measuring cylinder with a known volume of water to calculate their total volume via the volume change. The porosity calculations of the materials were obtained using the Pycnometer and the density data were obtained by comparing the theoretical density to the measured density:

$$\rho_{t=}\rho_{m} \times F_{m} + \rho_{r} \times F_{r} \tag{4}$$

$$P = \left(1 - \frac{\rho_e}{\rho_t}\right) \times 100\% \tag{5}$$

where ρ_t is the theoretical density; ρ_e is the experimental density, ρ_m (1.161 g/cm³) and ρ_r (1.30 g/cm³) are the SMV and the regolith simulant densities, respectively; F_m and F_r are the volume fraction of the SMV matrix and regolith particles, respectively; P is the porosity.

Characterizations

PANalytical Epsilon 3^{XLE} X-ray fluorescence (XRF) was used to determine the chemical composition of the regolith simulant. The results were compared to the real lunar soil to verify the analogy.

The cross-section of the SMV-regolith composite and the morphology of the regolith were analyzed using a Phenom ProX Desktop Scanning Electron Microscope (SEM) with an acceleration voltage of 15 KV. Prior to SEM imaging, the composite samples were sputtered with a layer of 10 nm gold to improve surface conductivity and reduce charging effects.

PerkinElmer Spectrum Two Fourier Transfer Infrared Spectroscopy (FTIR) was used to analyze the curing state of the 3D-printed composites. The compositional analyses of

the BPAGMA monomer, the 3D-printed pure vitrimer control sample, and the composite (20 wt% of regolith) were conducted using PerkinElmer Spectrum Two by collecting 32 scans with a scanning range of 4000-400 cm⁻¹.

TGA550 Thermogravimetric Analysis (TGA) was used to determine the degradation of the polymer and the 3D-printed regolith composite as a function of temperature. The weight loss of the composite and the polymer was analyzed as the samples were heating up. The weight loss and the derivative thermogravimetry (DTG) with respect to temperature are plotted.

Results and discussions

Lunar regolith simulant characterization

Table 1 shows the chemical composition of the lunar regolith simulant used in this work compared to real Apollo lunar regolith samples. SiO₂ and Al₂O₃ are the major components of the lunar regolith. The chemical composition of the lunar regolith simulant (LRS) used as the feedstock in this research is relatively similar to the real Apollo lunar soil and hence serves as a potential application for lunar-based construction.

SEM images of the Lunar Regolith Simulant (LRS) show micromorphology with angular random-size-and-shaped particles (Figure 2(a)–(c)). It is noted that some regolith particles are needle shaped. Because they have a small aspect ratio, they cannot function as short fibers, which usually reinforce the polymer matrix. Instead, the needle-shaped particles lead to reduced load-carrying capacity.

Mechanical behavior

Figure 3 shows the typical stress-strain curve of the vitrimer regolith composite where the compressive strength and the amount of elongation are summarized in Table 2. From the compressive test, the vitrimer control sample showed a higher compressive strength (200.7 \pm 2.28 MPa) than the regolith-filled composite. At room temperature, the polymer exhibited a linear elastic strain of up to 10% strain, after which it started yielding. Shortly after yielding, the curve remained horizontal or plastic flow between 12 and 17%, and the compressive stress of the polymer increased sharply afterward due to strain hardening. High brittleness and a decrease in compressive strength were observed in the composite as the amount of regolith in the composite increased. The decrease in the compressive strength with an increase in the regolith amount in the composite may be attributed to the high porosity caused by the irregularly shaped lunar regolith simulant and the weak interfacial bonding between the polymer matrix and the lunar regolith fillers. More importantly, the irregularly shaped regolith particles serve as stress concentration centers, leading to

Table 1. Chemical composition of various lunar samples a

Item	SiO ₂	Al_2O_3	TiO ₂	FeOT	MnO	MgO	CaO	Na ₂ O	K ₂ O	P ₂ O ₅
Apollo 14	47.97	17.57	1.77	10.41	0.14	9.18	11.15	0.7	0.5	0.52
Apollo 16	45.00	27.30	0.54	5.10	0.30	5.70	15.70	0.46	0.17	0.11
LRS	49.12	26.29	0.63	3.20	0.06	2.86	13.52	2.55	0.34	0.17

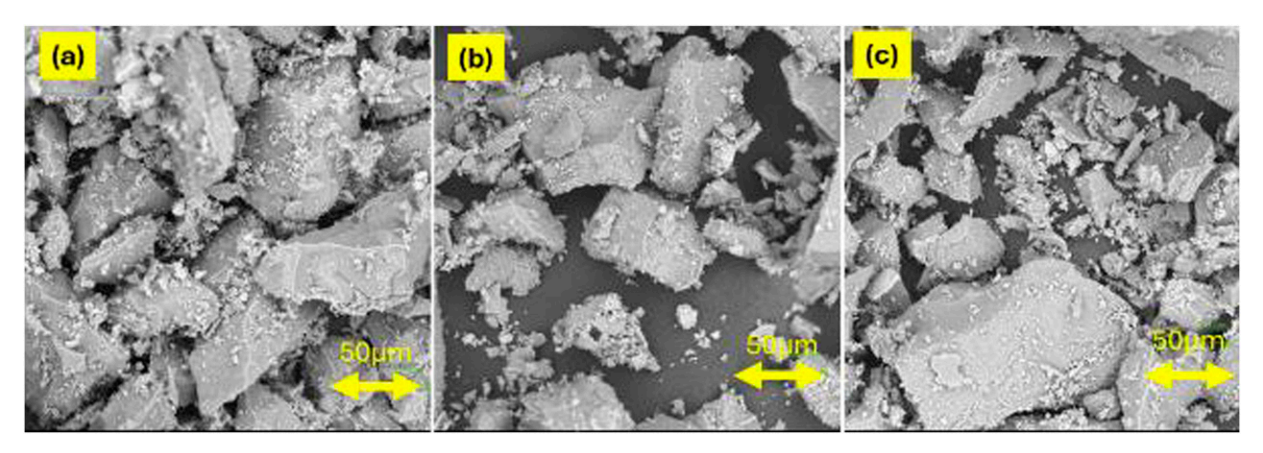


Figure 2. SEM images of regolith, which show loose micromorphology with sharp edges and jagged contour (a, b, c).

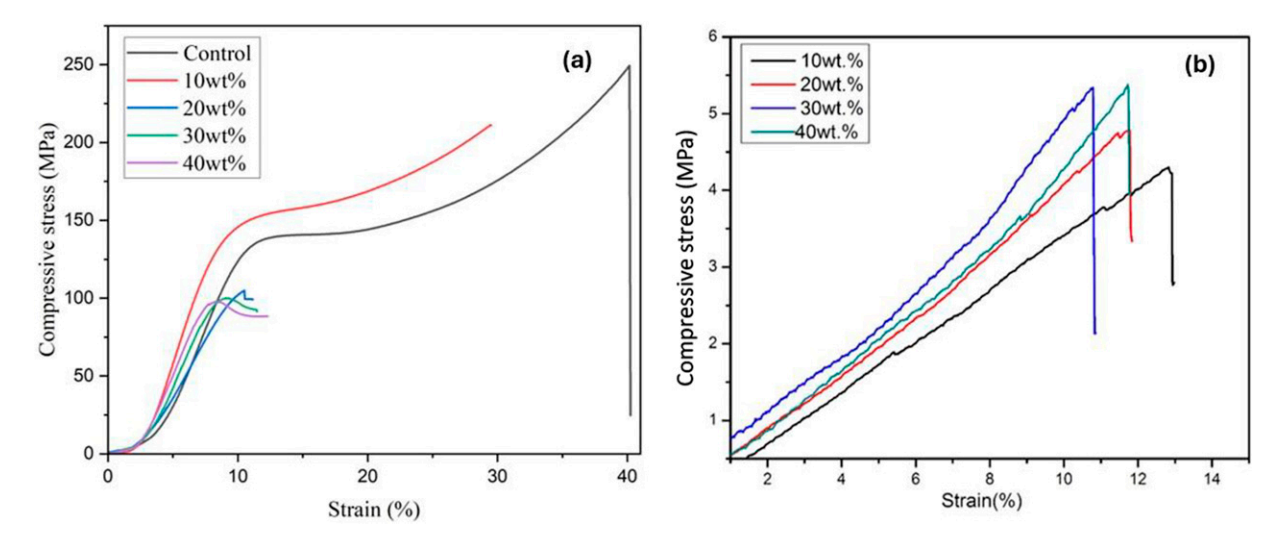


Figure 3. Stress-strain curve of SMV-regolith composite under compression: at room temperature (a), and at 190°C (b).

Table 2. Compressive strength of vitrimer regolith composite at room and elevated temperature.

Regolith (wt.%)	Compressive strength at room temperature	Compressive strength at elevated temperature (190°C)	Percentage increase in the compressive strength of the composites at elevated temperature (%)
Control (0)	200.7 ± 2.28	18.78 ± .34	_
10	185.5 ± 4.45	4.29 ± 0.55	_
20	102 ± 1.55	4.79 ± 0.20	11.65
30	99 ± 3.6	5.34 ± 0.28	11.48
40	96 ± 3.12	5.39 ± 0.75	0.94

premature failure at the particle/matrix interface. The composite containing 20, 30, and 40 wt% regolith undergoes linear elastic strain ranging from 11% to 13% before fracturing. In the Earth, the compressive strength of structural elements needed to withstand external loading, which includes external load and gravitational force, is typically in the range of 30 to 40 MPa. Given that the Moon has a lower gravitational force than the Earth—about one-sixth of Earth's gravitational force, the compressive strength of the polymeric lunar composite is high enough to withstand external loading, or approximately 70 MPa more than what would be required to load a given mass on Earth.

To further explain the effect of porosity on compressive strength in Figure 3(a) and Table 2, the porosity test results are summarized in Table 3. From Tables 3 and it is seen that with the increase in the regolith weight fraction, the porosity increases. One possible reason is that the regolith particles are irregularly shaped and have many sharp corners. This feature increases the friction and interlocking between particles during specimen preparation, resisting settlement of the particles in the SMV matrix, and leaving larger porosity. As a result, the compressive strength of the composites decreases as the weight fraction of the regolith particles increases. One possible solution is that a vibration table is used during specimen preparation process to pack the regolith particles densely.

The measurement results can be further validated by SEM observation. Figure 4 shows the SEM observation of the composites with different regolith weight fractions. It is seen that with the increase in the regolith weight fraction, the number of pores increases, and the pore size tends to become bigger. As a result, the compressive strength of the composites decreases as the regolith weight fraction increases.

At elevated temperatures, the polymer control sample shows a compressive strength of 18.78 MPa. From Figure 3(b), the compressive strength of the composite increases at high temperatures as the regolith weight fraction increases in the composite. This may be attributed to the transition of the polymer matrix from the glassy state to the rubbery state 45 and suggests that the polymer that had been softened at a high temperature was permitted to seep through the pores created by the lunar regolith simulant particles in the mixture as seen in the SEM images in Figure 5. This allows the polymer to fill in these pores and simultaneously bind the particles to form a concrete matrix, which is likely to result in a notable increase in strength. Another reason is that at high temperatures, the composite can be treated as hard particles dispersed in a soft matrix. As a result, the particles show a certain reinforcing effect, similar to hard particle-reinforced rubbers. Furthermore, zero yielding was recorded in the composite material at the elevated temperature which is due to the rubbery state of the SMV matrix.

Table 3. The density and porosity of the SMV-regolith composites.

Regolith (wt.%)	$ ho_{ m t}$ (g/cm 3)	$ ho_{\rm e}~({ m g/cm^3})$	Porosity (%)	
10	1.1749	1.137 ± 00.02	3.226	
20	1.1888	1.097 ± 00.08	7.722	
30	1.2027	1.079 ± 00.15	9.454	
40	1.2166	1.075 ± 00.25	10.570	

From the above discussions, it is seen that several factors affect the stress-strain behavior, as shown in Figure 3. More experimental studies such as more samples with different regolith weight fractions are needed to fully understand the coupling effect of porosity, pore size, and the number of pores on the stress-strain behavior.

Impact test results

Mechanical properties of the SMV-Regolith composites with glass fiber as hybrid reinforcement were analyzed under a low-velocity impact test. From Figure 6 and Table 4, it is seen that the laminate made of glass fabricreinforced pure SMV, or the control laminate, shows 0.62 ± 0.19 kN and 0.97 ± 0.34 J for the maximum impact load and crack initiation energy, respectively, as compared to the laminates made of glass fabric-reinforced SMV-regolith with impact load and crack initiation energy of 1.10 ± 0.05 kN and 1.82 ± 0.15 J respectively. The lower impact load and initiation energy are evidence of lower impact resistance. This suggests that the control laminate has lower bending strength, which is validated by three-point bending test results in Figure 7 and summarized in Table 5. One reason is that the glass fabricreinforced SMV-regolith composite has slightly higher stiffness than that of the control laminate, as shown in Figure 7 with a slightly larger slope in the stress-strain curves for the glass fabric-reinforced SMV-regolith composite laminates. The difference comes from the incorporation of regolith particles. The SMV-regolith composite, as a particulate-filled composite with relatively stiffer particles dispersed in a relatively softer matrix, has higher stiffness than the pure SMV matrix, based on the rule-of-mixture's prediction. The slightly higher bending stiffness translates to higher peak impact force, and higher initiation energy in the glass fabricreinforced SMV-regolith composite laminates. However, the propagation energy of the control laminate is lower than that of the glass fabric-reinforced SMV-regolith composite laminates, suggesting that the control laminate suffered from smaller damage from the impact event. This is understandable because the regolith particles in the SMV-regolith composite matrix serve as stress concentration centers, similar to other particulate-filled

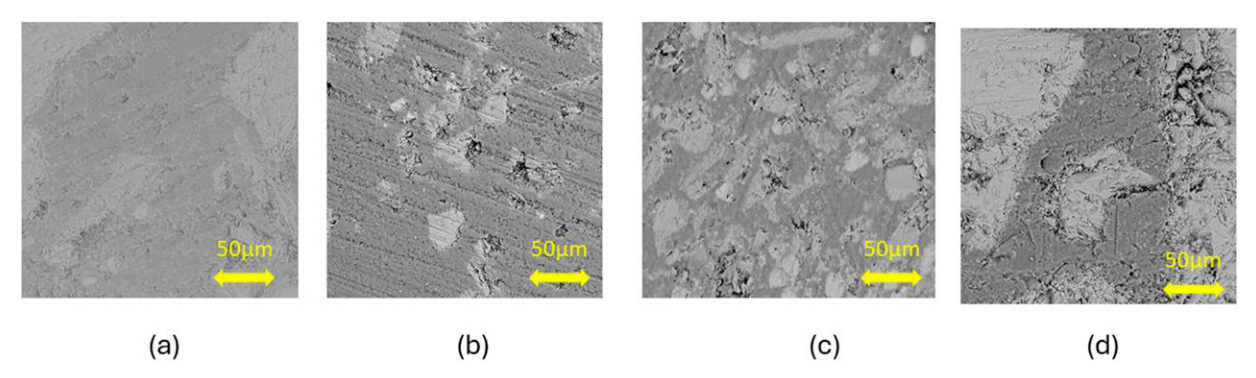


Figure 4. SEM images of SMV-regolith composites with different regolith weight fractions. From the SEM images the composite with 10 wt% regolith (a) has the least porosity. Higher porosity can be seen in the composite with higher regolith weight fraction. 20 wt% (b), 30 wt% (c), 40 wt% and (d).

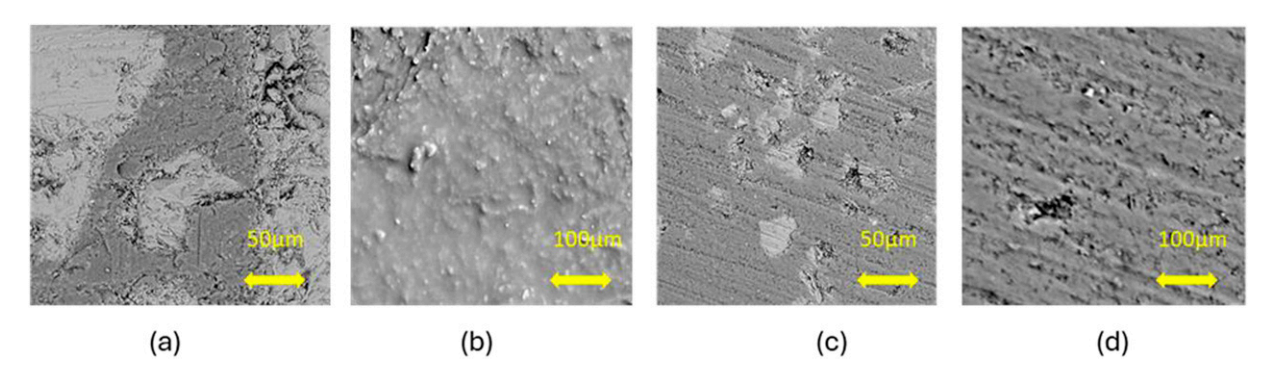


Figure 5. SEM images of composite under different testing conditions. (a) Composite with 40 wt% regolith ratio tested at room temperature, (b) composite with 40 wt% regolith ratio after elevated temperature mechanical test, (c) Composite with 20 wt% regolith ratio tested at room temperature, and (d) composite with 20 wt% regolith ratio tested at elevated temperature.

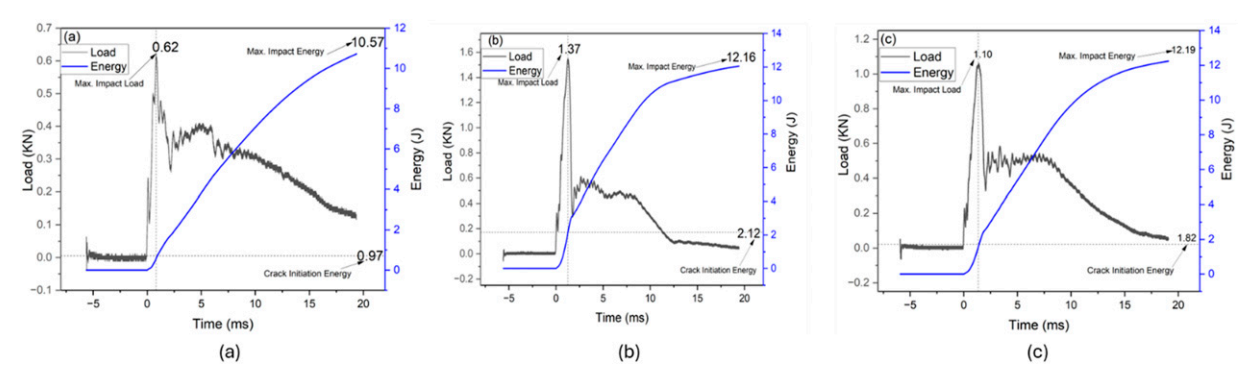


Figure 6. Graph of load and energy traces of low-velocity test: (a) Control glass fabric reinforced SMV composite laminate, (b) Glass fabric reinforced SMV-Regolith laminate composite with 20 wt% regolith fraction, (c) Glass fabric reinforced SMV-Regolith laminate composite with 40 wt% regolith fraction.

composites.⁵³ The stress concentration at the SMV/ regolith interface may cause matrix cracking and interfacial debonding, leading to more damage and more energy dissipation, or higher propagation energy. This can be

further validated by the slightly higher propagation energy for the laminate with 40 wt% regolith than that for the laminate with 20 wt% of regolith because more regolith particles translate to a larger potential for damage.

 Table 4. Mechanical Properties of Composite Laminate based on three-point bending and low-velocity impact tests.

Sample	Max impact force (KN)	Max impact energy (J)	Initiation energy (J)	Propagation energy (J)	Flexural strength (MPa)
Control	0.62 ± 0.19	10.57 ± 0.36	0.97 ± 0.34	9.60 ± 0.09	136.07 ± 6
20 wt%	1.37 ± 0.03	12.16 ± 0.43	2.12 ± 0.59	10.03 ± 0.61	222.15 ± 8
40 wt%	1.10 ± 0.05	12.19 ± 0.10	1.82 ± 0.15	10.38 ± 0.08	232.70 ± 5

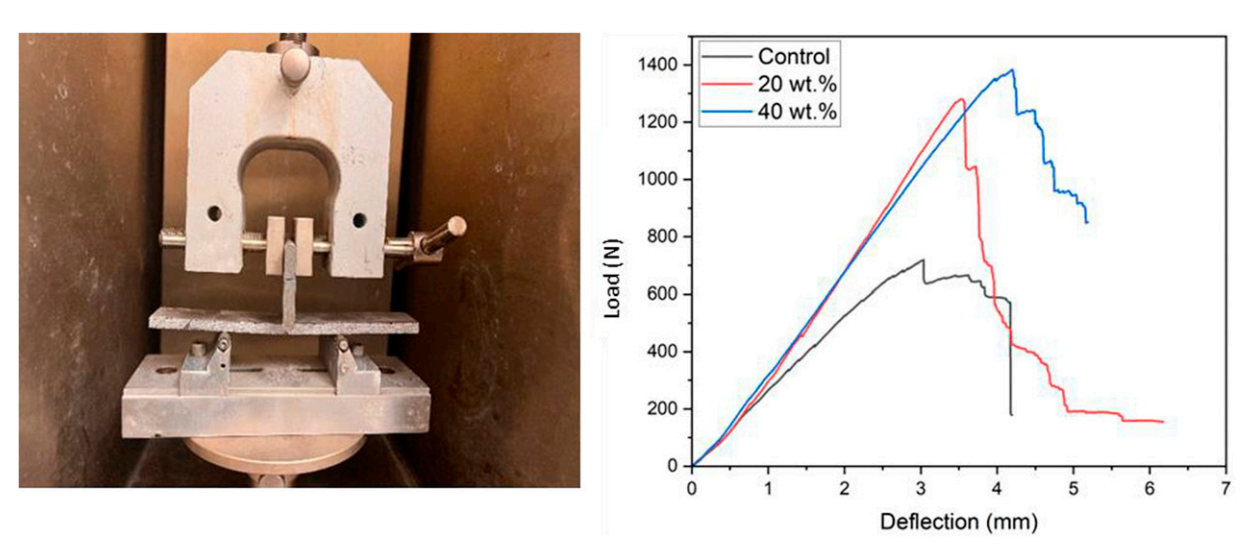


Figure 7. Glass fabric reinforced SMV and SMV-regolith laminated composites under a three-point bending test.

Table 5. Summary of mechanical properties and healing efficiency after each healing cycle.

	Healing cycle	Healing efficiency (%)				
Regolith ratio (wt. %)		Based on crack initiation energy	Based on crack propagation energy	Based on maximum impact load		
Control	ı	99.03 ± 0.57	99.22 ± 0.22	84.5 ± 0.24		
	2	75.03 ± 1.34	83.39 ± 1.41	55.61 ± 163		
20%	ı	97.4 ± 0.65	91.93 ± 1.15	80.82 ± 2.3		
	2	88.68 ± 1.52	91.64 ± 1.5	62.16 ± 1.75		
40%	ı	92.29 ± 0.96	88.99 ± 1.22	39.4 ± 2.3		
	2	79.31 ± 1.5	71.99 ± 1.7	31.91 ± 2.3		

Healing efficiency of the composites

The major advantage of using SMV as the binder for the lunar regolith is the self-healing, recyclable, and reprocesseable properties of the vitrimer. Li et al. 45 demonstrated the recyclability of the SMV that was used as the matrix for the composite material in this work. The self-healing efficiency of the SMV was computed by comparing the mechanical properties of the recycled vitrimer to that of the original vitrimer. Li et al. 45 in their work recorded a healing efficiency of 69.5% and 62.1% for the first and second healing cycles, respectively. Konlan et al. 46 incorporated conductive shape memory alloy wires and

employed the closed-then-heal (CTH) healing method proposed by Li et al. ^{51,52} in healing their SMV laminated composite. A healing efficiency of 100% and 99.24% for the first and second healing cycles was achieved, respectively. Zhang and Li⁴⁹ also used polymeric artificial muscles to serve as embedded sutures to close wide-opened cracks, which can be fabricated through twist insertion in precursor fibers such as fibers with negative coefficient of thermal expansions or two-way shape memory polymers. ⁵⁰

In this work, the closed-then-heal method was employed in the healing of the SMV-regolith laminated composite. The composite was healed at an elevated temperature of

150°C under a compressive pressure of 16 MPa. The healing efficiency was computed using the data obtained from the second and third impact tests after two healing cycles. From Tables 5 and it is observed that an increase in the regolith ratio in the composite led to a decrease in the healing efficiency of the composite. This may be caused by the excess regolith particles that interfere with the reconfiguration of the broken bonds in the SMV chains during the healing process. It was also confirmed that the healing efficiency of the composite decreases as the number of damage/healing cycles increases. Furthermore, the calculated healing efficiency changes depending on the criterion used. Clearly, using peak impact force as the criterion, the healing efficiency is lowest, that is, the most conservative.

Properties of 3D-Printed SMV-regolith composites

3D printing results. In this study, the SMV-regolith composite was printed using a Liquid Crystal Display (LCD) type of 3D printer. Figure 8 shows structures with very simple to very complex shapes that have been printed successfully. The 3D printability of the SMV-regolith composite makes it a potential candidate for construction on the Moon.

FTIR characterization results. Figure 9 shows the FTIR results of a 3D-printed SMV-regolith composite. The FTIR results show the presence of Biphenol A unit (1450 cm⁻¹), Ester bonds (1735 cm⁻¹), C = C double bonds (1600 cm⁻¹), and hydroxyl groups (3200 cm⁻¹ – 3600 cm⁻¹) in the BPAGMA monomer. The result from the test shows the

direct chemical information about the double-bond conversion. The strength of the particulate composite depends on the degree of curing of the 3D-printed parts. FTIR analysis shows the complete breakdown of the double bonds in the BPAGMA monomer into stronger single bonds after curing. This shows the complete curing of the composite.

Thermal analysis. Figure 10 shows that both the SMV and the SMV-regolith composite have thermal stability up to 300 °C. Temperature at 5% weight loss $T_{(5\%)}$ occurred at 301 °C and 329 °C for the composite and SMV, respectively. Minimal weight loss of 0.5% occurred at 180°C which is the post-thermal curing temperature after the 3D printing. Thus, post-thermal curing of the printed sample does not have any significant effect on the material degradation.

From Figure 10, the sample exhibited a 2-step degradation pattern. (1) Both the SMV and the printed composite lost 3% and 5% of their original weight, respectively, from the starting temperature of 23 °C to a temperature of 300 °C, which may be due to dehydration of solvent materials and absorbed moisture. (2) The second major dehydration occurred between 330°C and 507°C, which is equivalent to an 85% decrease in original weight. This was due to the depolymerization, dehydration, and decomposition of the SMV which results in the formation of char. Considering that the temperature on the surface of the Moon is much lower than the decomposition temperature of the SMV-regolith composite, it is expected that structures 3D printed using the composite are thermally stable on the surface of the Moon.

Shape memory effect of the 3D printed SM-regolith composites. The shape memory effect of the 3D-printed



Figure 8. 3D printed SMV-regolith composite samples using LCD printer.

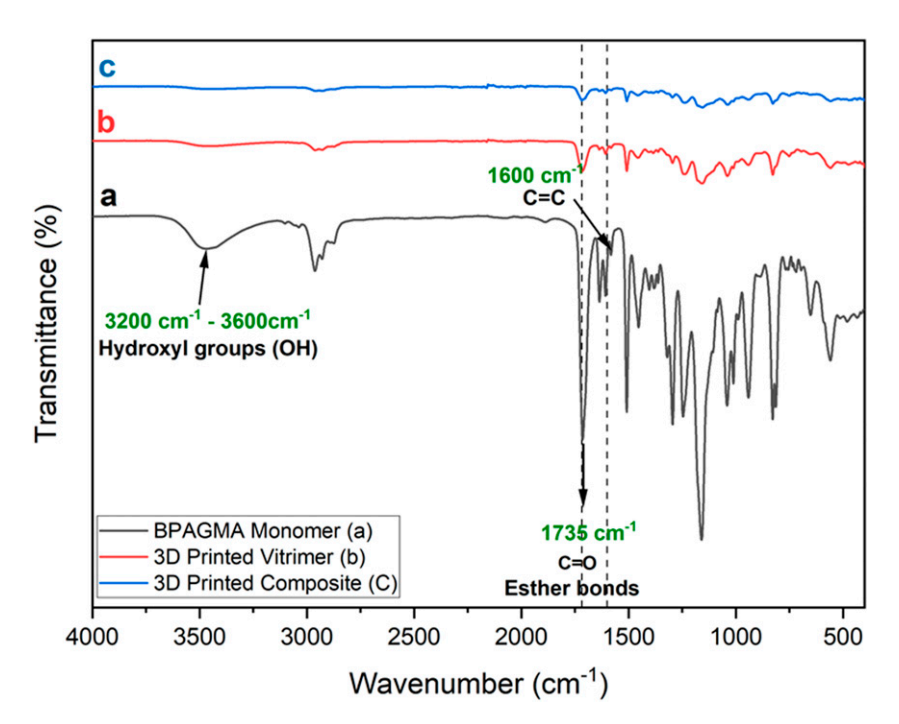


Figure 9. FTIR spectrum of 3D printed SMV, SMV-regolith composite samples, and BPAGMA resin signifying the complete curing of the printed samples.

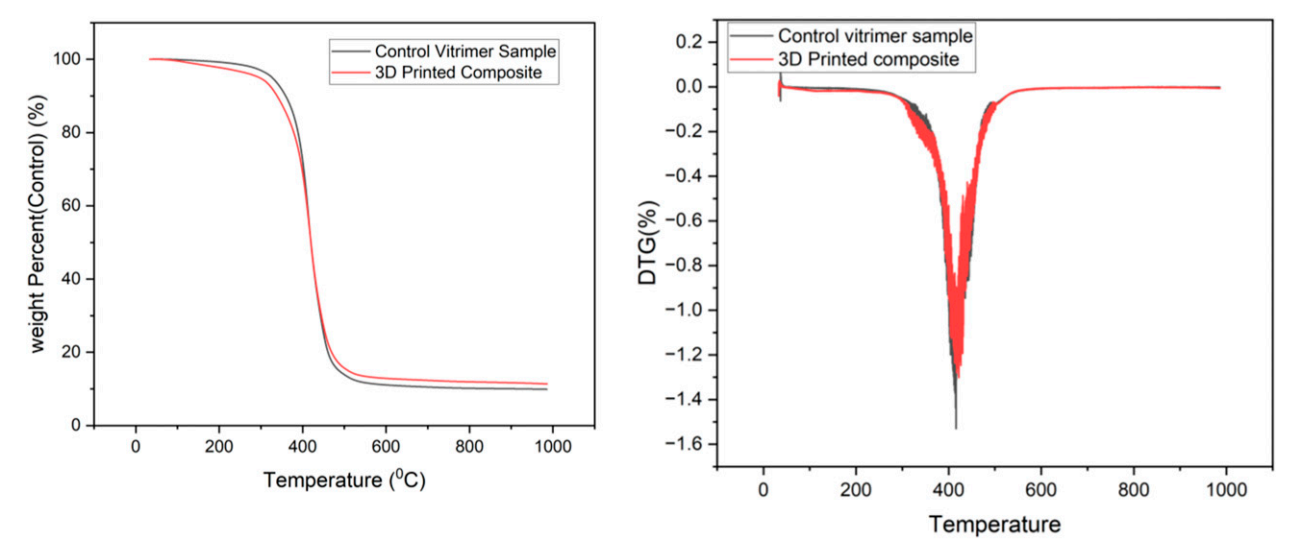


Figure 10. TG and DTG curves of 3D printed vitrimer (SMV) and SMV-regolith composites.

SMV-regolith composite was evaluated. Shape memory properties of the composite were investigated via its shape fixity ratio and free shape recovery ratio. The 3D printed composite was first programmed by following 4-step procedures, including (1) Heating the system; (2) Loading at rubbery temperature; (3) Cooling to a glassy state while holding the stress constant; and (4) Unloading. In this study, a 3D printed composite cylinder of diameter 11.22 mm and

height of 34.16 mm was compressed by the MTS machine until 5% strain was attained at a temperature of 140°C in an oven which was pre-heated for 1h. The system was immediately cooled to prevent the motion of the polymer chain segments and fix the temporary shape. After unloading, the compression programming was completed. After that, the programmed sample was reheated back to 140°C, without applying any constraint, and the recovery strain was

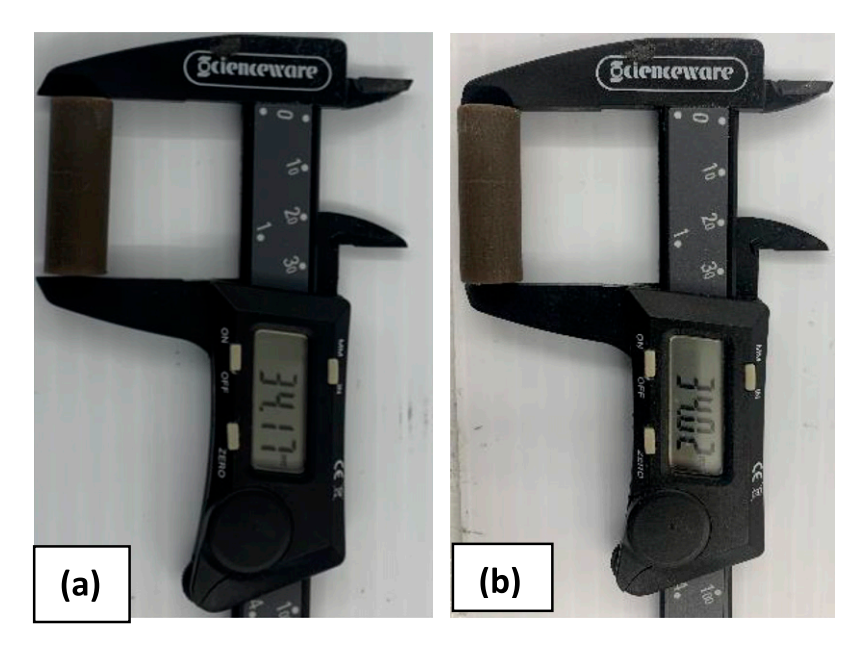


Figure 11. (a) The initial height of the specimen (b) the height of the specimen after free shape recovery.

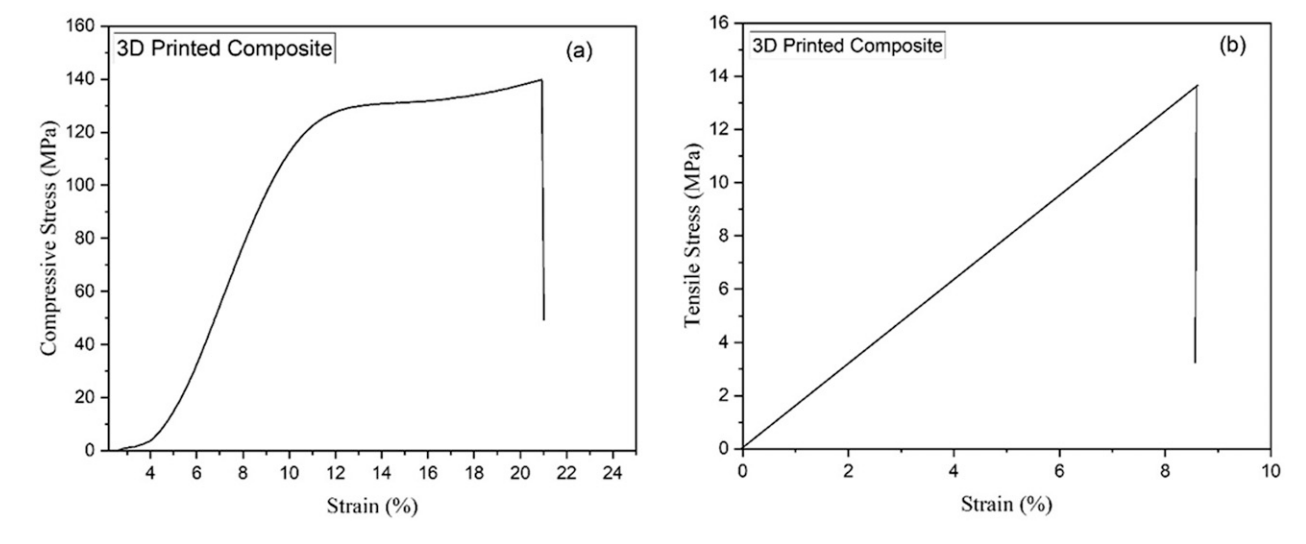


Figure 12. (a) Typical room temperature compressive stress versus strain curve of the 3D printed cylindrical specimens obtained from compression test at a loading rate of 1 mm/min. (b) Typical tensile stress versus strain curves of the 3D printed dogbone specimens obtained from the tensile test at room temperatures with a loading rate of 1 mm/min.

recorded. The shape fixity ratio (F) and the shape recovery ratio (R) were determined based on the measured heights of the sample during programming and free shape recovery, using the following equations:

$$\frac{h_0 - h_2}{h_0 - h_1} \times 100\tag{6}$$

$$\frac{h_3 - h_2}{h_0 - h_2} \times 100\tag{7}$$

where h_0 = initial height of the cylinder, h_1 = height after compression, h_2 = height after load removal, and h_3 = height after shape recovery. The composite exhibited a good shape recovery property, with a shape fixity ratio (F) of 68.88 \pm 1.35% and a shape recovery ratio (R) of 88.20 \pm 1.28% based on the test results of four samples. Figure 11 shows the various heights were measured using a caliper.

Mechanical properties of the 3D printed SMV-regolith composites. 3D-printed cylindrical and dogbone-shaped

samples were used for the tensile and compressive tests, respectively. After printing, the samples were post-cured in an oven for 1h to attain uniformly cured samples. Five samples were used for the uniaxial mechanical tests. The compressive and tensile behavior of the printed composites were investigated at room temperature using an MTS QI5O machine with a loading rate of 1 mm/min. Figures 12(a) and (b) show the typical stress-strain behavior of the composite under compression and tension, respectively. From the compressive tests, the printed composite showed a compressive strength of 139.2 MPa. At room temperature, the composite exhibited a linear elastic strain of up to 10%, after which it started yielding. Shortly after yielding, the curve remained constant between 13 and 18%. A small increase in the magnitude of the compression stress was observed as a result of strain hardening before failure. The 3D-printed sample exhibited elastic behavior under tensile testing. No yielding was observed under tensile testing. The tensile strength was about 14 MPa, while the failure strain was about 8.4%, suggesting that the SMV-regolith composite is brittle under tension. This is typical for other concrete such as cement concrete.

Conclusions

In summary, a shape memory vitrimer regolith composite was synthesized using lunar regolith simulant and shape memory vitrimer as the constituent materials. Both the conventional synthesis and 3D printing technology were explored in the synthesis of the composite structures. Mechanical testing was performed on the composite with varied regolith ratios to evaluate the performance of the composites under different lunar conditions. The compression test reveals that an increase in the ratio of the regolith in the composite leads to a decrease in the mechanical properties of the composite in the glassy state. This is mainly caused by the lack of binder, the increase in porosity, and the increase in stress concentration, as evidenced by the SEM images. At the rubbery state, the compression test results show that the compressive strength increases as the particle weight fraction increases, most likely due to the reinforcing effect of the hard particles in a soft matrix. Glass fabric was also introduced to make hybrid composite laminate, which shows high flexural strength, high peak impact force, and high initiation energy, under low-velocity impact test. The composite laminate was healed, and the results show a high healing efficiency. 3D printing of the SMV-regolith composite samples was also conducted using a Liquid Crystal Display (LCD) printer. The printed samples exhibited good thermomechanical properties which is very essential considering the harsh lunar environment. Future space exploration and colonization call for the use of lunar resources and modern technology as ways to establish temporary and permanent settlements in the lunar environment. This work explored the use of sustainable materials and technology to achieve this goal in a resource-starved environment.

It is noted that this study did not consider the harsh lunar environment such as huge temperature gradient, high radiation, etc. More tests are needed to fully understand the suitability of this composite for lunar exploration. It is also important to note that the LCD-based printing using vatphotopolymerization has limited size in the printed samples. Extrusion based 3D printing may be more appropriate, which will be a topic for our future studies.

Declaration of conflicting interests

The author(s) declared no potential conflicts of interest with respect to the research, authorship, and/or publication of this article.

Funding

The author(s) disclosed receipt of the following financial support for the research, authorship, and/or publication of this article: This work was supported by the This work is supported by the NASA Cooperative agreement 80NSSC21M9266, the US National Science Foundation under grant number OIA-1946231 and the Louisiana Board of Regents for the Louisiana Materials Design Alliance (LAMDA), and the US National Science Foundation under grant number HRD-1736136.

ORCID iDs

John Konlan https://orcid.org/0000-0001-6136-4340 Guoqiang Li https://orcid.org/0000-0002-7004-6659

Data availability statement

The datasets generated during and/or analyzed during the current study are available from the corresponding author upon reasonable request.

References

- Jakus AE, Koube KD, Geisendorfer NR, et al. Robust and elastic lunar and martian structures from 3D-printed regolith inks. Sci Rep 2017; 7: 44931–44938. DOI: 10.1038/ srep44931.
- Fateri M and Gebhardt A. Process parameters development of selective laser melting of lunar regolith for on-site manufacturing applications. *Int J Appl Ceram Technol* 2015; 12: 46–52. DOI: 10.1111/ijac.12326.
- Bao C, Wang Y, Tahir Mushtaq R, et al. Preparation and characterization of elevated and cryogenic temperatureresistant regolith-based epoxy resin composites. *Construct Build Mater* 2023; 387: 131560. DOI: 10.1016/j. conbuildmat.2023.131560.
- Labeaga-Martínez N, Sanjurjo-Rivo M, Díaz-Álvarez J, et al. Additive manufacturing for a Moon village. *Procedia Manuf* 2017; 13: 794–801. DOI: 10.1016/j.promfg.2017.09.186.

 Zhou C, Chen R, Xu J, et al. In-situ construction method for lunar habitation: Chinese Super Mason. *Autom ConStruct* 2019; 104: 66–79. DOI: 10.1016/j.autcon.2019.03.024.

- Grossman KD, Sakthivel TS, Sibille L, et al. Regolith-derived ferrosilicon as a potential feedstock material for wire-based additive manufacturing. *Adv Space Res* 2019; 63: 2212–2219. DOI: 10.1016/j.asr.2018.12.002.
- Faierson EJ, Logan KV, Stewart BK, et al. Demonstration of concept for fabrication of lunar physical assets utilizing lunar regolith simulant and a geothermite reaction. *Acta Astronaut* 2010; 67: 38–45. DOI: 10.1016/j.actaastro.2009.12.006.
- 8. Miller J, Taylor L, Zeitlin C, et al. Lunar soil as shielding against space radiation. *Radiat Meas* 2009; 44: 163–167. DOI: 10.1016/j.radmeas.2009.01.010.
- Kornuta D, Abbud-madrid A, Atkinson J, et al. Commercial lunar propellant architecture: a collaborative study of lunar propellant production. *Reach Out* 2019; 13: 100026. DOI: 10. 1016/j.reach.2019.100026.
- Koelle DE. Cost efficiency as design and selection criterion for future launch vehicles. *Acta Astronaut* 2005; 57: 623–629.
 DOI: 10.1016/j.actaastro.2005.02.001.
- Weigel AL and Hastings DE. Evaluating the cost and risk impacts of launch choices. *J Spacecraft Rockets* 2004; 41: 103–110. DOI: 10.2514/1.9270.
- Jones HW. The recent large reduction in space launch cost. 48th international conference on environmental systems. New Mexico: Albuquerque, 2018. https://ntrs.nasa.gov/api/ citations/20200001093/downloads/20200001093.pdf.
- Balla VK, Roberson LB, Connor O, et al. First demonstration on direct laser fabrication of lunar regolith parts. *Rapid Prototyp J* 2012; 6: 451–457. DOI: 10.1108/13552541211271992.
- McLemore CA, Fikes JC, Darby CA, et al. Fabrication capabilities utilizing in situ materials, https://ntrs.nasa.gov/api/ citations/20090014085/downloads/20090014085.pdf 2008.
- 15. Naser MZ. Extraterrestrial construction materials. *Prog Mater Sci* 2019: 105: 100577. DOI: 10.1016/j.pmatsci.2019.100577.
- 16. Keller LP and Mckay DS. The nature and origin of rims on lunar soil grains. *Geochem Cosmochim Acta* 1997; 61: 2331–2341. DOI: 10.1016/S0016-7037(97)00085-9.
- Egnaczyk TM, Hartt V WH, Mills JN, et al. Compositionproperty relationships of BP-1 lunar regolith simulant geopolymers for in-situ resource utilization. *Adv Space Res* 2024; 73: 885–917. DOI: 10.1016/j.asr.2023.11.030.
- 18. Chen M, Lin H, Wen Y, et al. Construction of a virtual lunar environment platform. *International Journal of Digital Earth* 2013; 6: 469–482. DOI: 10.1080/17538947.2011.628415.
- Suescun-florez E, Roslyakov S, Iskander M, et al. Geotechnical properties of BP-1 lunar regolith simulant. *J Aero Eng* 2015; 28: 1–9. DOI: 10.1061/(ASCE)AS.1943-5525. 0000462.
- Farries KW, Visintin P, Smith ST, et al. Sintered or melted regolith for lunar construction: state-of-the-art review and future research directions. *Construct Build Mater* 2021; 296: 123627. DOI: 10.1016/j.conbuildmat.2021.123627.

 Simonds CH. Sintering-and-hot-pressing-of-fra-maurocomposition-glass-and-the-lithification-of-lunar-breccias, https:// ntrs.nasa.gov/citations/19730049073 1973.

- Hoshino T, Wakabayashi S, Yoshihara S, et al. Key technology development for future lunar utilization block production using lunar regolith. *Trans. JSASS Aerospace Tech. Japan* 2016; 14: 35–40. https://www.jstage.jst.go.jp/article/tastj/14/ists30/14 Pk 35/ pdf.
- 23. Fateri M, Cowley A, Kolbe M, et al. Localized microwave thermal posttreatment of sintered samples of lunar simulant. *J Aero Eng* 2019; 32: 1–7. DOI: 10.1061/(ASCE)AS.1943-5525.0001039.
- Noble S. The lunar regolith, https://www.nasa.gov/wp-content/uploads/2019/04/05_1_snoble_thelunarregolith.pdf 1980.
- Wang X and Pedrycz W. Petrologic characteristics of the lunar surface. Sci Rep 2015; 5: 17075. DOI: 10.1038/srep17075.
- Lee J, Ann KY, Lee TS, et al. Bottom-up heating method for producing polyethylene lunar concrete in lunar environment. *Adv Space Res* 2018; 62: 164–173. DOI: 10.1016/j.asr.2018. 03.039.
- Lee TS, Lee J and Yong K. Acta astronautica manufacture of polymeric concrete on the Moon. *Acta Astronaut* 2015; 114: 60–64. DOI: 10.1016/j.actaastro.2015.04.004.
- 28. Lee TS, Ann KY, Chul B, et al. Solidification of polymer concrete using the artificial lunar soil. *Earth Space* 2015; 2014: 283–290.
- Utekar S, V K S, More N, et al. Comprehensive study of recycling of thermosetting polymer composites – driving force, challenges and methods. *Composites Part B* 2021; 207: 108596. DOI: 10.1016/j.compositesb.2020.108596.
- Al-darkazali A, Çolak P, Kadıoğlu K, et al. Mechanical properties of thermoplastic and thermoset composites reinforced with 3D biaxial warp-knitted fabrics. *Appl Compos Mater* 2018; 25: 939–951. DOI: 10.1007/s10443-018-9725-x.
- Giorgini L, Benelli T, Brancolini G, et al. Recycling of carbon fiber reinforced composite waste to close their life cycle in a cradle-to-cradle approach. *Curr Opin Green Sustainable Chem* 2020; 26: 100368. DOI: 10.1016/j. cogsc.2020.100368.
- Alabiso W and Schlögl S. The impact of vitrimers on the industry of the future: chemistry, properties and sustainable forward-looking applications. *Polymers* 2020; 12: 1660. DOI: 10.3390/polym12081660.
- Zhang Y, Zhang L, Yang G, et al. Recent advances in recyclable thermosets and thermoset composites based on covalent adaptable networks. *J Mater Sci Technol* 2021; 92: 75–87. DOI: 10.1016/j.jmst.2021.03.043.
- 34. Wu Y, Wei Y and Ji Y. Carbon material/vitrimer composites: towards sustainable, functional, and high-performance crosslinked polymeric materials. *Giant (Oxf)* 2023; 13: 100136. DOI: 10.1016/j.giant.2022.100136.
- Gelino NJ Selection, production, and properties of regolith polymer, https://ntrs.nasa.gov/citations/20230015024.

- Taylor SL, Jakus AE, Koube KD, et al. Sintering of microtrusses created by extrusion-3D-printing of lunar regolith inks. *Acta Astronaut* 2018; 143: 1–8. DOI: 10.1016/j. actaastro.2017.11.005.
- Yang W, Zhao W, Li Q, et al. Fabrication of smart components by 3D printing and laser-scribing technologies. ACS Appl Mater Interfaces 2020; 12: 3928–3935. DOI: 10.1021/ acsami.9b17467.
- 38. Goulas A and Friel RJ. 3D printing with moondust. *Rapid Prototyp J* 2016; 22: 864–870. DOI: 10.1108/RPJ-02-2015-0022.
- 39. Wong JY and Pfahnl AC. 3D printing of surgical instruments for long-duration space missions. *Aviat Space Environ Med* 2014; 85: 758–763. DOI: 10.3357/ASEM.3898.2014.
- Cesaretti G, Dini E, De Kestelier X, et al. Building components for an outpost on the Lunar soil by means of a novel 3D printing technology. *Acta Astronaut* 2014; 93: 430–450. DOI: 10.1016/j.actaastro.2013.07.034.
- Liu M, Tang W, Duan W, et al. Digital light processing of lunar regolith structures with high mechanical properties. *Ceram Int* 2019; 45: 5829–5836. DOI: 10.1016/j.ceramint.2018.12.049.
- 42. Dou R, Tang WZ, Wang L, et al. Sintering of lunar regolith structures fabricated via digital light processing. *Ceram Int* 2019; 45: 17210–17215. DOI: 10.1016/j.ceramint.2019.05.276.
- 43. Tibbits S. 4D printing: multi-material shape change. *DES* 2014; 84: 116–121. DOI: 10.1002/ad.1710.
- Ge Q, Dunn CK, Qi HJ, et al. Active origami by 4D printing. *Smart Mater Struct* 2014; 23: 094007. DOI: 10.1088/0964-1726/23/9/094007.
- 45. Li A, Fan J and Li G. Recyclable thermoset shape memory polymers with high stress and energy output: via facile UV-curing. *J Mater Chem A* 2018; 6: 11479–11487. DOI: 10. 1039/c8ta02644k.

- Konlan J, Mensah P, Ibekwe S, et al. A laminated vitrimer composite with strain sensing, delamination self-healing, deicing, and room-temperature shape restoration properties.
 J Compos Mater 2022; 56: 2267–2278. DOI: 10.1177/00219983221098225.
- Konlan J, Mensah P, Ibekwe S, et al. Vitrimer based composite laminates with shape memory alloy Z-pins for repeated healing of impact induced delamination. *Composer Part B* 2020; 200: 108324. DOI: 10.1016/j.compositesb. 2020.108324.
- Li A, Challapalli A and Li G. 4D printing of recyclable lightweight architectures using high recovery stress shape memory polymer. *Sci Rep* 2019; 9: 7621–7623. DOI: 10. 1038/s41598-019-44110-9.
- Zhang P and Li G. Healing-on-demand Composites Based on Polymer Artificial Muscle. *Polymer*. 2015; 64: 29–38. DOI: 10.1016/j.polymer.2015.03.022.
- Fan J and Li G. High performance and tunable artificial muscle based on two-way shape memory polymer. *RSC Advances*. 2017; 7(2): 1127–1136. DOI: 10.1039/C6RA25024F.
- Li G and Nettles D. Thermomechanical characterization of a shape memory polymer based self-repairing syntactic foam. *Polymer* 2010; 51: 755–762. DOI: 10.1016/j.polymer.2009.12. 002.
- Li G and Uppu N. Shape memory polymer based self-healing syntactic foam: 3-D confined thermomechanical characterization. *Compos Sci Technol* 2010; 70: 1419–1427. DOI: 10. 1016/j.compscitech.2010.04.026.
- Li G, Zhao Y and Pang SS. Analytical modeling of particle size and cluster effects on particulate-filled composite. *Mater Sci Eng* 1999; 271: 43–52. DOI: 10.1016/S0921-5093(99) 00227-0.